 https://doi.org/10.3311/PPch.42157

Periodica Polytechnica Chemical Engineering, 69(4), pp. 632–648, 2025

Quantifying the Stability–defect–layer Trade-off in Surfactant-assisted Fluid-dynamic Exfoliation of Few-layer Graphene

Amun Amri[1*], Deki Sarma[1], Panca Setia Utama[1], Dhina Febryza[1], Mohammednoor Altarawneh[2], Khairulazhar Jumbri[3], Hatem Taha[4], Hussein A. Miran[5], Zainab N. Jaf[5], Mohammad Mahbubur Rahman[6], Mazhibayev Assylzhan[7], Zhong Tao Jiang[4]

[1] Department of Chemical Engineering, Faculty of Engineering, University of Riau, Bina Widya Campus KM. 12.5, 28293 Pekanbaru, Indonesia
[2] Chemical and Petroleum Engineering Department, College of Engineering, United Arab Emirates University, P. O. B. 15551, Abu Dhabi, United Arab Emirates
[3] Department of Applied Science, Faculty of Science, Management & Computing, Universiti Teknologi Petronas, 32610 Seri Iskandar, Perak, Malaysia
[4] Surface Analysis and Materials Engineering Research Group, School of Engineering and Information Technology, Murdoch University, South St. 90., 6150 Murdoch, WA, Australia
[5] Department of Physics, College of Education for Pure Science (Ibn Al-Haitham), University of Baghdad, Al-Jadriya, P. O. B. 4732, 10071 Baghdad, Iraq
[6] Department of Physics, Jahangirnagar University, Kalabagan Rd. 138., 1342 Savar, Dhaka, Bangladesh
[7] Department of Chemistry and Chemical Technology, Faculty of Technology, Taraz University named after M.Kh. Dulaty, Suleymenov 7., 080000 Taraz, Kazakhstan
[*] Corresponding author, e-mail: amun.amri@eng.unri.ac.id

Received: 08 September 2025, Accepted: 26 November 2025, Published online: 17 December 2025

Abstract

In this paper we report an all-aqueous fluid-dynamic exfoliation route to low-defect few-layer graphene (FLG) using the non-ionic surfactant Triton X-100. Systematic variation of surfactant concentration (1–5 wt%) and processing time (0.5–1.5 h) revealed a quantitative interplay among stability, defect, and layer. Raman spectroscopy and 2D band Lorentzian modeling revealed that the few-layer graphene (FLG) predominantly consists of four layers, with very low defect ratios (I_D/I_G = 0.02–0.11; I_{2D}/I_G = 0.18–0.30). Raman imaging confirmed spatially uniform G band intensity, while the edge-activated D band signals indicated residual edge defects characteristic of shear-cleaved flakes. Transmission electron microscopy and particle size analysis yielded lateral sizes of ~1.29–1.43 μm with a narrow distribution. Fourier transform infrared spectroscopy verified that the defects were not oxidation-derived, while UV–Vis showed graphene π–π absorption at 270–276 nm. This work establishes a short-duration, low-cost, and solvent-free approach for producing stable FLG suitable for liquid-phase applications and provides process–structure metrics for benchmarking across exfoliation studies.

Keywords

few-layer graphene (FLG), fluid-dynamic exfoliation (FDE), surfactant concentration, exfoliation time, characterizations

1 Introduction

Graphene exhibits significant potential for diverse applications due to its outstanding physical, chemical, and mechanical attributes. Its notable specifications include a tensile strength of 130 GPa, a Young's modulus of 1 TPa, a specific surface area of 2630 $m^2\ g^{-1}$, thermal conductivity of approximately 5000 $W\ m^{-1}\ K^{-1}$, and electronic mobility of up to 200,000 $cm^2\ V^{-1}\ s^{-1}$ [1–3]. Graphene has been utilized in various fields, including advanced composites, battery additives, supercapacitors, solar cells, membranes, photocatalysts, flexible sensors, and more [4, 5]. The main obstacle in fabricating this material lies in producing high-quality defect-free and few-layer graphene (FLG) on a large scale [6]. Researchers encounter significant obstacles due to restricted production capacity and elevated manufacturing expenses [7].

Various techniques have been established to generate superior, defect-free graphene, such as chemical vapor deposition, epitaxial growth, and organic production [1]. However, these bottom-up approaches have notable drawbacks, including high production costs, energy-intensive

Cite this article as: Amri, A., Sarma, D., Utama, P. S., Febryza, D., Altarawneh, M., Jumbri, K., Taha, H., Miran, H. A., Jaf, Z. N., Rahman, M. M., Assylzhan, M., Jiang, Z. T. "Quantifying the Stability–defect–layer Trade-off in Surfactant-assisted Fluid-dynamic Exfoliation of Few-layer Graphene", Periodica Polytechnica Chemical Engineering, 69(4), pp. 632–648, 2025. https://doi.org/10.3311/PPch.42157

processes, the use of toxic materials and volatile solvents, and relatively low yields compared to top-down methods [8–10]. Several top-down methods have been developed, including liquid-phase exfoliation [11, 12], shear exfoliation [13], microfluidization, Taylor-Couette, and thin-film reactors [14, 15], most of which can produce defect-free graphene without oxidation. Liquid-phase exfoliation, a top-down technique, is considered effective for large-scale graphene fabrication due to its simplicity and relatively low production costs. In practical applications, liquid-phase graphene is particularly useful, as it can be homogeneously dispersed in materials to enhance performance compared with solid-phase (powder) graphene [16].

According to Guardia et al. [17], producing graphene via liquid-phase exfoliation using ionic surfactants can yield monolayer or few-layer graphene with basal planes largely free of structural flaws and at low cost [17]. However, excessively high concentrations of ionic surfactants are reported to reduce the graphene yield. Increasing the ionic surfactant concentration reduces the potential barrier and enhances van der Waals forces, resulting in graphene instability [18]. Yi and Shen [19] reported that graphene could be synthesized from graphite via exfoliation in a rotating blade mixer for 8 h using N,N-dimethylformamide (DMF) as the working fluid. Although the resulting graphene exhibited an average thickness of less than five layers and defect-free basal planes, the solvent is highly volatile and expensive. Furthermore, the produced graphene exhibits irregular configurations [19].

Varrla et al. [12] successfully synthesized graphene nanosheets from graphite powder using turbulence-assisted shear exfoliation (TASE) in a rotating blade mixer, utilizing water as the solvent and a blend of anionic and non-ionic surfactants. The resultant graphene was defects-free, averaging approximately 6 layers with an average lateral dimension of 630 nm. The method utilized in this study is notably simple and cost-effective, making it beneficial for extensive production. Nonetheless, the synthesized graphene exhibited a comparatively elevated number of layers [12]. Further innovation was introduced by Amri et al. [20], who combined two exfoliation processes: an initial stage in a rotating blade mixer followed by a high-shear mixing. This approach produced defect-free graphene predominantly consisting of 1–3 layers, with a lateral size of approximately 375.4 nm [20]. However, using the anionic surfactant sodium lauryl sulfate (SLS) in this study exhibited lower stability than non-ionic surfactants [21].

Girish and Tambe [22] effectively produced graphene using liquid-phase mechanical exfoliation technique with a rotating blade mixer. Graphite flakes were exfoliated in distilled water with Tween 80 as a surfactant. The resulting graphene consisted of 3–8 layers with high purity and defect-free basal planes. However, the graphene synthesis process required a prolonged duration of approximately 10 h, rendering the method less efficient [22]. Wang et al. [21] evaluated the contribution of surfactant type and concentration on graphene fabrication through liquid-phase exfoliation utilizing an ultrasonic system [21]. The graphene concentration rose with surfactant addition, but later diminished due to sheet aggregation caused by excessive surfactant. The non-ionic surfactant Triton X-100 exhibited outstanding stability performance. However, the ultrasonic system in this study was less efficient due to its high energy cost and long processing time (8 h) [21].

In light of these limitations, this study established an all-aqueous fluid-dynamic exfoliation (FDE) approach that systematically correlates surfactant concentration and processing time with graphene quality metrics. Unlike previous reports requiring organic solvents, mixed surfactant systems, or prolonged durations of ≥8–10 h, our method demonstrated that a simple rotating-blade hydrodynamic field operating in water with Triton X-100 delivered low-defect, FLG (~4 layers) in only 1.5 h. Beyond achieving short-duration and solvent-free exfoliation, we provided quantitative correlations between surfactant concentration, Raman defect ratios (I_D/I_G), layer numbers (from 2D band deconvolution), lateral size distributions, and suspension stability. Furthermore, we reported hydrodynamic descriptors to enhance reproducibility and benchmarking across studies. This combination of rapid processing, environmentally benign medium, and quantitative process–structure–property mapping established a distinct advancement over previous exfoliation works and offers a scalable, cost-effective, and replicable pathway for producing liquid-dispersible graphene suitable for next-generation nanomaterial applications.

2 Materials and methods

2.1 Preparation of graphene

Graphene was synthesized from pure graphite (Tianjin Dingshenxin Chemical Industry Co. Ltd) using the FDE process in a rotating blade mixer (kitchen blender) with water containing the non-ionic surfactant Triton X-100 (Merck) as the working fluid. The surfactant concentration was at 1 wt%, 3 wt%, and 5 wt%, and the FDE durations were 0.5,

1, and 1.5 h. The resulting black liquid was allowed to settle for 24 s, after which the graphene solution was separated from the sediment [12]. The solution was then dried in an oven at 60 °C for 24 h to obtain graphene powder.

2.2 Characterizations

The raw graphite and manufactured graphene were analyzed using Raman spectroscopy (RS), Raman imaging (RI), transmission electron microscopy (TEM), Fourier transform infrared spectroscopy (FTIR) with attenuated total reflectance (ATR) technique, UV-Vis spectroscopy, and particle size analysis (PSA). RS and RI analyses were conducted using the WITec Alpha 300R Raman spectrometer (WITec GmbH, Ulm, Germany) with molecular vibrations stimulated by a 532 nm wavelength laser. The 2D peak was analyzed via Lorentzian peak fitting using OriginPro software [23]. The morphology and dimensions of graphene were identified using a TEM HT7700 (Hitachi High Technologies America, Inc., Schaumburg, IL, USA) instrument, and TEM images were processed using ImageJ software [24]. PSA was conducted using the dynamic light scattering technique with a Malvern Zetasizer Nano ZS (Malvern Panalytical Ltd., UK) to ascertain the particle size distribution of graphene. FTIR analysis was performed to ascertain the functional groups present in graphene utilizing a Nicolet iS10 instrument (Thermo, USA). UV-Vis spectroscopy was performed with a PerkinElmer Lambda 35 UV/VIS Spectrometer (PerkinElmer, USA), with graphene powder suspended in deionized water to identify the absorption peaks of the synthesized graphene samples.

3 Result and discussion

3.1 Raman spectroscopy

Fig. 1 presents the Raman spectra of the pristine graphite (particle size 5 μm) and the graphene synthesized via the FDE process using a rotating blade mixer. The working fluid comprises water containing the surfactant Triton-X at varying concentrations (1–5 wt%). Different FDE processing times Fig. 1 (a) 0.5 h, Fig. 1 (b) 1 h and Fig. 1 (c) 1.5 h were applied. The Raman spectrum of graphite exhibits three characteristic peaks: the D band (1363.8 cm^{-1}), G band (1584.2 cm^{-1}), and 2D band (2718.2 cm^{-1}). Peaks within these regions identify graphite [25]. The low intensity of the D band peak indicates that the graphite precursor has few defects.

In Fig. 1, each sample demonstrates a G band peak position displaced toward lower Raman shift regions relative to that of pristine graphite (~1584.2 cm^{-1}). This shift initially indicates the exfoliation of graphite into mono- or multilayer

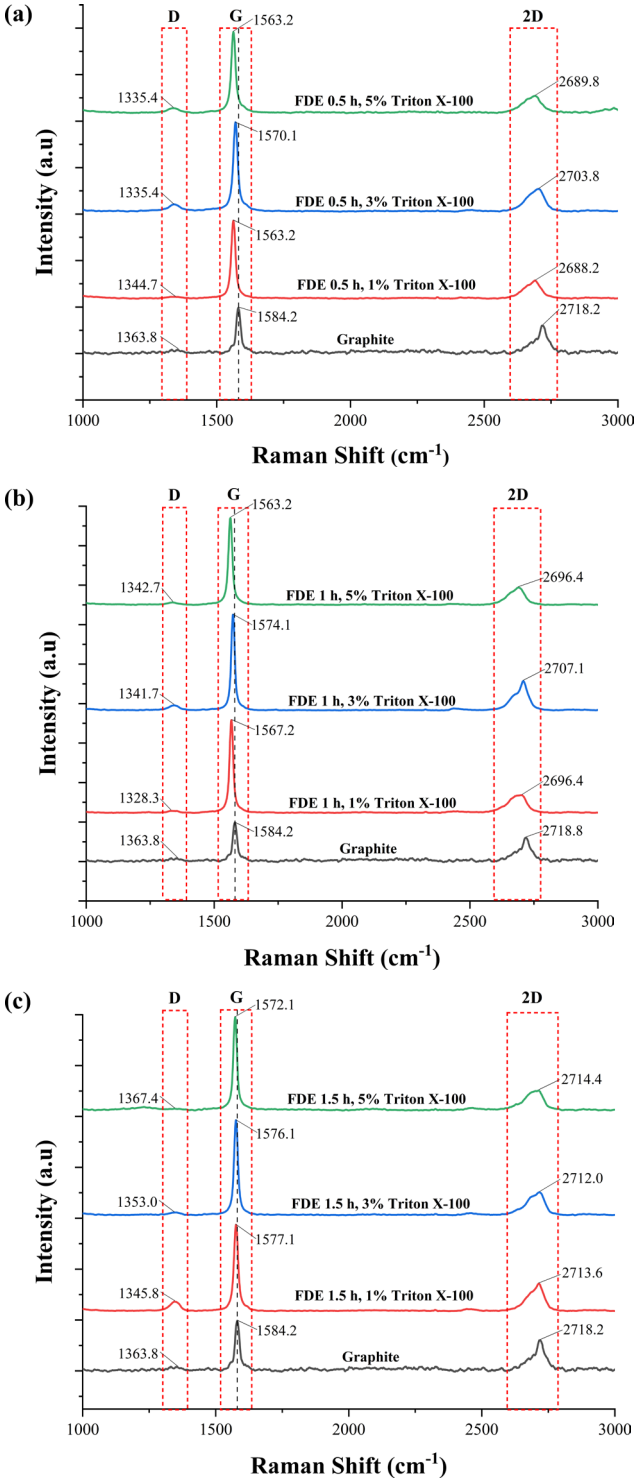

Fig. 1 Raman spectra of pristine graphite and FDE graphene at varying FDE processing times: (a) 0.5 h, (b) 1 h and (c) 1.5 h

graphene [20, 26]. The G band arises from first-order Raman scattering of doubly degenerate in-plane vibrational modes (transverse and longitudinal optical phonons) at the Brillouin zone center [20, 26, 27]. In addition to the G band, the 2D band appears, which is sensitive to the number of graphene layers. The 2D band results from second-order

Raman scattering of in-plane transverse optical phonons near the Brillouin zone boundary and is closely associated with the electronic band structure [27].

Fig. 1 (a)–(c) shows that each sample exhibits a broadened and asymmetric 2D band peak. The 2D band is also associated with double-resonance transitions that produce two phonons with opposite momentum [28]. A distinct, acute, and robust 2D peak is characteristic of single-layer graphene (SLG), while bilayer graphene (BLG) and FLG exhibit asymmetric and broadened peaks as the number of layers increases. This broadening occurs due to additional electronic branches resulting from interlayer electronic interactions, contributing to the Raman spectrum [26, 29]. As the layer number increases, the electrical band structure undergoes splitting, further widening the 2D band [26–28, 30]. Fig. 1 (a)–(c) also shows that the 2D band peaks exhibit asymmetric broadening, attributed to additional electronic branches caused by electron-phonon scattering, which generates multiple Raman peaks in the 2D band spectrum for four-layer graphene (4LG) and multilayer graphene (>4LG) [20, 26, 29].

In Fig. 1, the Raman spectra of graphite and prepared graphene show no distinct D′ and D + G disturbance peaks, signifying that the FDE exfoliation process did not induce substantial flaws in the graphene. However, the presence of a D band peak in the Raman spectrum indicates that the produced graphene is not entirely defect-free. The D band arises from transverse optical phonons near the Brillouin zone corner and results from the six-membered carbon ring vibrations in graphene, requiring defects for activation [20, 27, 31]. The observed defects (indicated by the D band peak) in Fig. 1 are not due to oxidation (such as hydroxyl, carboxyl, or epoxy groups) because the inert nature of mono- or multilayer graphene and the high surfactant concentration prevent oxidation during exfoliation [21]. The defects are attributed to edge imperfections generated during the shear exfoliation process using the rotating blade mixer, reducing graphene lateral size [19].

In Fig. 1 (a)–(c), the D band peak intensity decreases with advancing concentrations of the Triton X-100 surfactant, indicating a reduction in graphene defects. This result aligns with studies by Guardia et al. [17] and Wang et al. [21], who reported that elevated concentrations of the non-ionic surfactant Triton X-100 enhance graphene concentration until reaching saturation (at the highest level). The increased graphene concentration indicates high dispersion stability of exfoliated graphene in aqueous solutions. During exfoliation, vacancy defects may form in graphene layers due to carbon atom loss caused by particle collisions and shear forces. These processes can break carbon bonds in regions under pressure, collisions, or friction [32]. These vacancy defects are believed to contribute to the splitting of graphene into smaller lateral sizes [33], leading to smaller graphene lateral sizes and reduction or elimination of vacancy defects [17, 21, 34]. However, the increase in D band intensity at a 3 wt% surfactant concentration relative to graphite (0.6 mg mL^{-1}) is attributed to decreased graphene stability. Wang et al. [21] reported a decline in graphene concentration at surfactant concentrations above 0.5 mg mL^{-1}. Exfoliated graphene requires binding with surfactant molecules that generate steric repulsion forces to prevent re-aggregation. Insufficient surfactant molecules result in weaker steric repulsion than the van der Waals forces between exfoliated graphene layers, causing graphene aggregation and reduced stability. Lower stability also indicates more reactive sites in graphene due to edge and vacancy defects [21, 35]. Further analysis of the 2D band Raman peaks using Lorentzian peak fitting was performed with OriginPro software [23], as presented in Fig. 2.

Fig. 2 illustrates the Lorentzian peak fitting results for the 2D band of RS from graphene and graphite samples obtained using OriginPro software [23]. In Fig. 2, the raw graphite material reveals two Lorentzian components [20, 26]. The Lorentzian peak fitting results for the 2D band peaks of each sample during the FDE process (0.5–1.5 h) and at varying Triton X-100 surfactant concentration (1 wt%, 3 wt%, and 5 wt%) demonstrate three and two Lorentzian components, respectively. These findings align with those of Malard et al. [26] and Amri et al. [20], indicating that the presence of three Lorentzian components in the 2D band peak corresponds to graphene dominated by four layers, while two Lorentzian components indicate multilayer graphene (>4 layers) [20, 26, 30].

Table 1 summarizes the intensity ratios of the D band to the G band (I_D/I_G) and the 2D band to the G band (I_{2D}/I_G). The synthesized graphene exhibits I_D/I_G ratios extending from 0.02 to 0.11 and I_{2D}/I_G ratios from 0.18 to 0.30. Comparisons of the I_{2D}/I_G and I_D/I_G peaks in Table 1 classify the synthesized graphene as FLG. Zhang et al. [25] and Nguyen et al. [36] indicated that an I_{2D}/I_G intensity ratio below 1 is characteristic of FLG. Huang et al. [37] and Phiri et al. [38] reported that an I_D/I_G intensity ratio below 0.3 corresponds to FLG dominated by approximately 3–5 layers. The defect level in graphene can be quantified by examining the I_D/I_G ratio [20, 39]. An increased I_D/I_G ratio indicates the exfoliation of graphite into graphene, attributed to the formation of new edges (edge defects) during exfoliation, which produces smaller graphene flakes. Consequently, smaller flakes have a higher edge-to-volume ratio [17, 34].

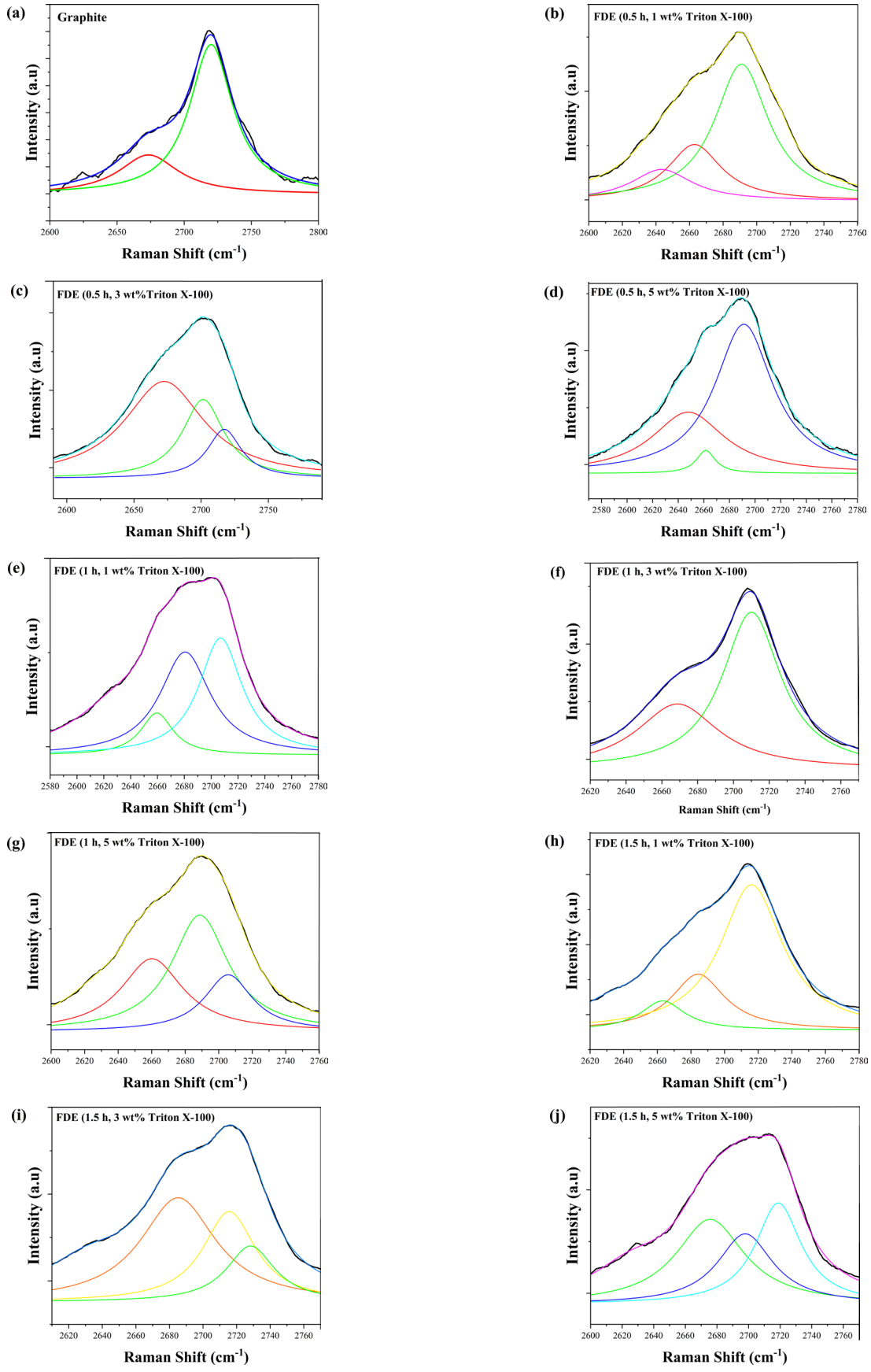

Fig. 2 Lorentzian peak fitting of 2D Raman spectrum bands using 532 nm laser excitation: (a) Graphite, (b) FDE (0.5 h, 1 wt% Triton X-100), (c) FDE (0.5 h, 3 wt% Triton X-100), (d) FDE (0.5 h, 5 wt% Triton X-100), (e) FDE (1 h, 1 wt% Triton X-100), (f) FDE (1 h, 3 wt% Triton X-100), (g) FDE (1 h, 5 wt% Triton X-100), (h) FDE (1.5 h, 1 wt% Triton X-100), (i) FDE (1.5 h, 3 wt% Triton X-100), (j) FDE (1.5 h, 5 wt% Triton X-100)

Table 1 I_D/I_G and I_{2D}/I_G intensity ratios

FDE process duration (h)	Triton X-100 (wt%)	I_D/I_G	I_{2D}/I_G
	1	0.03	0.22
0.5	3	0.08	0.24
	5	0.06	0.20
	1	0.03	0.18
1	3	0.05	0.28
	5	0.03	0.19
	1	0.11	0.30
1.5	3	0.03	0.23
	5	0.02	0.21

Table 1 reveals that at a Triton X-100 concentration of 1 wt%, the I_D/I_G ratio increases with longer FDE processing times. Conversely, at Triton X-100 concentrations of 3 wt% and 5 wt%, the I_D/I_G ratio decreases with extended FDE durations. This behavior is attributed to higher concentrations of non-ionic surfactants, where prolonged exfoliation enhances graphene dispersion in aqueous solutions. As the FDE duration increases, the quantity of exfoliated graphene rises due to turbulence and shear forces. With sufficient surfactant, the dispersed graphene remains stable [17, 34]. The best results were obtained for the sample processed for 1.5 h with 5 wt% Triton X-100 surfactant, characterized by four-layer graphene consistent with Lorentzian peak analysis (3 peaks) and low defect levels, showing the lowest I_D/I_G ratio at the same layer number (I_D/I_G ratio of 0.02).

3.2 Solution stability analysis

Fig. 3 illustrates the visual stability tests of graphene suspensions synthesized using the FDE method for 0.5–1.5 h with Triton X-100 surfactant concentrations ranging from 1 wt% to 5 wt%. In the figure, black and opaque suspensions indicate good graphene stability, while non-black or transparent suspensions signify poor stability due to graphene agglomeration and sedimentation [17, 40]. Fig. 3 illustrates that using 1 wt% Triton X-100 and an FDE processing time of 1.5 h produces a more transparent suspension than samples processed for 0.5–1 h, indicating reduced stability. The decreased stability arises because prolonged FDE processing (1.5 h) increases collisions between graphene particles, generating more exfoliated fragments. The low concentration of Triton X-100 (1 wt%) is inadequate to inhibit aggregation due to the weak steric repulsion offered by the surfactant [40].

Fig. 3 demonstrates that increasing the surfactant concentration to 3–5 wt% produces darker suspensions as the FDE processing time increases, indicating improved graphene stability. This observation aligns with the I_D/I_G ratio comparison in Table 1, where the I_D/I_G ratio decreases with longer FDE processing times. A lower I_D/I_G ratio suggests a decline in defects within the graphene structure, reducing reactive edges and enhancing graphene stability in aqueous solutions [34]. Prolonged FDE processing with adequate surfactant concentrations results in better graphene dispersion and stability. The black and opaque appearance of the suspension signifies minimal defects in the graphene, reducing the likelihood of aggregation due to fewer reactive edges [17, 40].

3.3 Raman imaging

Fig. 4 presents the optical and Raman images of the FLG sample (1.5 h, 5 wt% surfactant). In Fig. 4 (a), the arrangement of luminous yellow specks against a darker backdrop signifies variations in the material's intensity or optical characteristics. The findings indicate that the luminous areas in Fig. 4 (b) correlate with the emergence of the G band, exhibiting a uniform distribution of G band intensity across the graphene sheet, implying the superior quality of the synthesized graphene [31]. This finding is further supported by the Raman spectra obtained at point 1 (Fig. 4 (c)) and point 2 (Fig. 4 (d)), demonstrating that brighter colors in the Raman image correspond to higher charge-coupled device (CCD) counts. Fig. 4 (c), (d) displays three distinctive peaks of graphene: the D band (~1367 cm^{-1}), the G band (~1572 cm^{-1}), and the 2D band (~2714 cm^{-1}). The brighter colors indicate regions with higher G band peak intensity, where greater G band intensity correlates with thicker graphene layers [41–43]. As graphene thickness increases (indicating more layers), the Raman signal intensity also rises, directly enhancing the number of photons captured by the CCD. This results in higher CCD counts, as observed in the Raman spectrum peaks [43]. RI is essential for determining graphene chirality and significantly determining its intrinsic properties, especially for various implementations [20]. The properties of graphene, including its magnetic, electrical, optical, electronic, mechanical, and chemical characteristics, are significantly influenced by edge chirality (zigzag or armchair) [31, 44].

Fig. 5 demonstrates the Raman image analysis of the FLG sample (1.5 h, 5 wt% surfactant) derived from the D band intensity. The arrangement exhibits a hexagonal blue-patterned illustration, forming angles of 30°, 120°, and 150°, with two adjacent edges identified as either armchair or zigzag [31]. The D band observed at armchair edges is significantly stronger than at zigzag edges [20, 31]. This finding aligns with Malard et al. [26], who reported

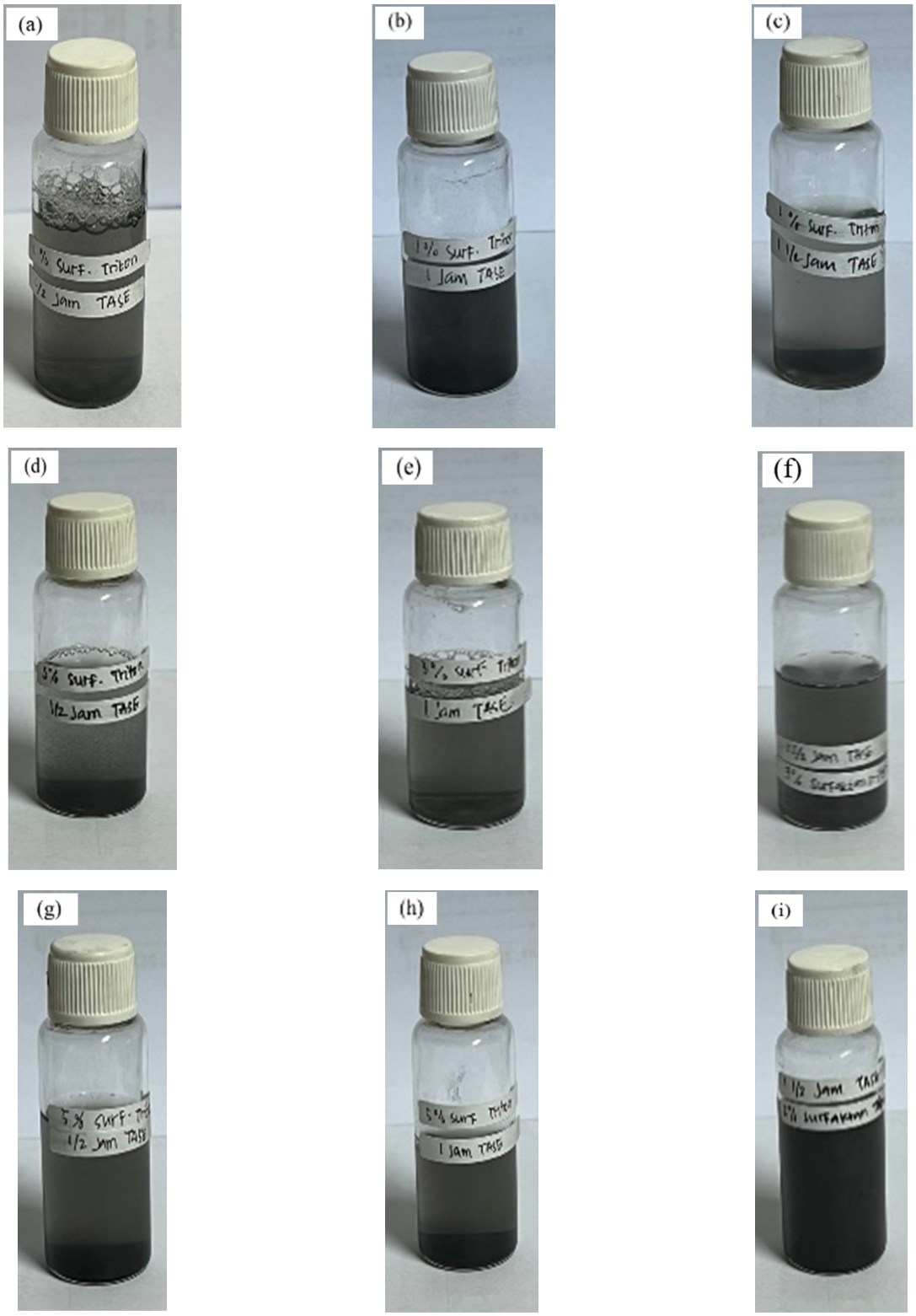

Fig. 3 Stability of graphene suspensions after 72 h with varying concentrations of Triton X-100 and FDE times: (a) 1 wt%, 0.5 h; (b) 1 wt%, 1 h; (c) 1 wt%, 1.5 h; (d) 3 wt%, 0.5 h; (e) 3 wt%, 1 h; (f) 3 wt%, 1.5 h; (g) 5 wt%, 0.5 h; (h) 5 wt%, 1 h; (i) 5 wt%, 1.5 h

that only armchair edges, rather than zigzag edges, are expected to display the D band in Raman spectra. In Fig. 5, angles of 60° and 120° are visible, corresponding to identical edge chirality (carbon atom arrangements at the edges), either armchair or zigzag. This aligns with You et al. [31], who stated that when the angle formed between two adjacent sides is 60° or 120°, both sides exhibit the same chirality, whether zigzag or armchair [31]. A 150° angle is also observed, consisting of one armchair and one zigzag side. This also aligns with the findings of You et al. [31],

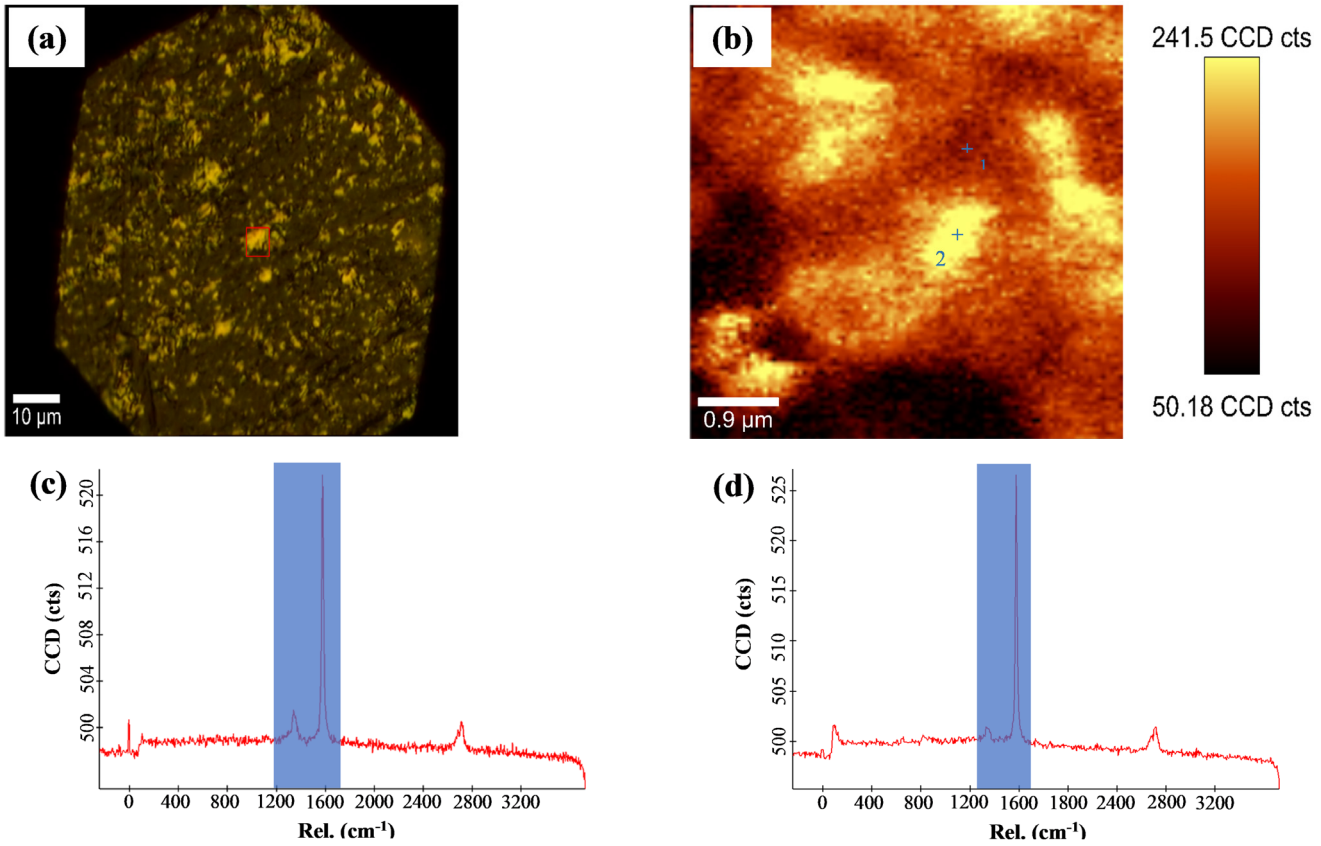

Fig. 4 Illustrates the FLG sample (1.5 h, 5 wt% surfactant), where (a) is the optical image, (b) is the Raman image constructed based on the G band intensity, (c) shows the Raman spectrum taken at point 1, and (d) presents the Raman spectrum taken at point 2

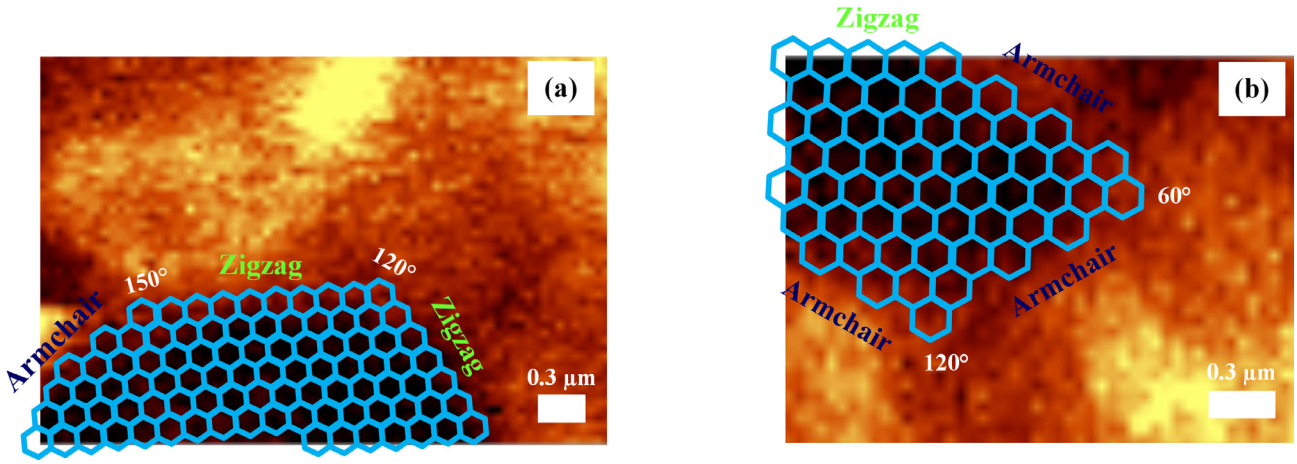

Fig. 5 Raman image of FLG (1.5 h, 5 wt% surfactant) constructed based on the D band intensity, with the expected arrangement in blue (angles ~60°, 120°, 150°)

which demonstrate that when the angles formed are 30°, 90°, or 150°, the chirality of the two adjacent sides differ, with one being a zigzag edge and the other an armchair edge [31]. According to You et al. [31] and Malard et al. [26], an increasing proportion of zigzag structures indicates higher-quality, defect-free graphene with fewer reactive edges. Conversely, a higher proportion of armchair structures suggests more defects (edge imperfections) in graphene [26, 31]. Fig. 5 clearly shows that armchair edges dominate over zigzag edges, explaining the existence of the D band in the Raman spectrum of FLG (1.5 h, 5 wt% surfactant). Thus, it can be concluded that FLG synthesized using the FDE process for 1.5 h with 5 wt% Triton-X surfactant still contains edge defects.

3.4 Transmission electron microscopy

Fig. 6 displays TEM images of FLG obtained from the FDE process conducted for 1.5 h with 5 wt% Triton-X 100 surfactant (Fig. 6 (b)) and graphite as a reference sample (Fig. 6 (a)). In Fig. 6 (a), graphite consists of many stacked graphene layers with large lateral size [20]. Conversely, Fig. 6 (b) demonstrates that the exfoliated graphene sheets are significantly thinner, exhibiting nanometer-scale thickness and reduced lateral dimensions [12, 20]. The graphene sample comprises several overlapping layers, confirming the RS results. The bright and dark regions in Fig. 6 (b) represent the layered structure of FLG [13, 20, 45]. Additionally, Fig. 6 (b) reveals smooth edges, highlighted by four black lines, indicating that the graphene structure predominantly comprises 4-layer graphene (4LG) [13, 20]. The magnified red box in Fig. 6 (b) reveals aggregates, likely formed due to the stabilizing agent Triton-X 100 surfactant [20]. The hydrophobic tails of the surfactant molecules are adsorbed onto the graphene flakes, whilst the hydrophilic segments extend into the aqueous medium, creating steric hindrance [46]. An insufficient number of surfactant molecules reduces the steric repulsive forces around the graphene surface, lowering the energy barrier compared with the van der Waals forces between graphene layers, thus leading to particle aggregation [20, 21, 35].

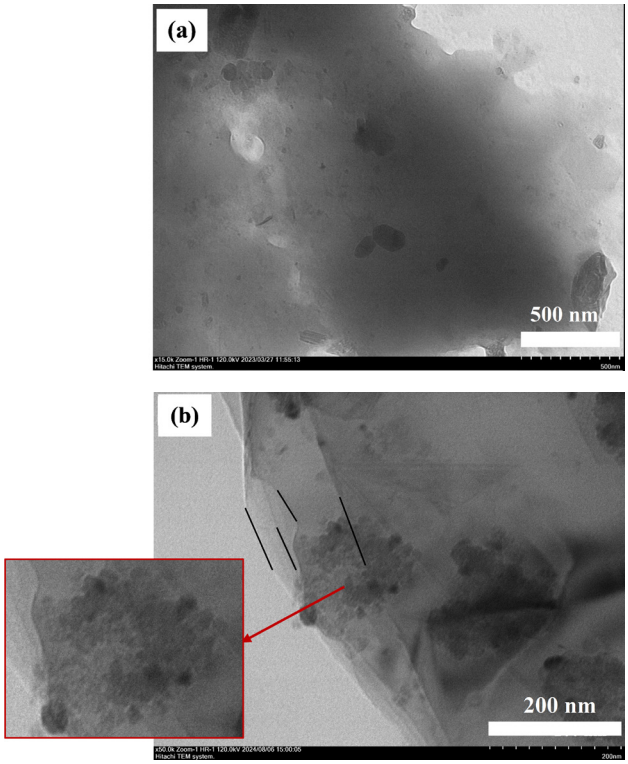

Fig. 6 TEM analysis results: (a) Graphite and (b) FLG (1.5 h, 5 wt% surfactant)

Fig. 7 presents the histogram of flake length distribution for FLG (1.5 h, 5 wt% surfactant). The flake lengths of FLG were estimated through image processing via the ImageJ software [12, 20, 24, 47]. The average flake length of the prepared FLG sample was 1288.98 ± 1048.80 nm. A total of 40 probes were measured. This result closely aligns with the average lateral size of FLG synthesized by Lotya et al. [48], approximately 1.2 µm [48]. Similarly, Khan et al. [49] stated that liquid-phase exfoliation can produce FLG with a mean lateral size of 1.1 µm [49]. The reduction in average flake length compared with the raw graphite material (5 µm) indicates that graphite was effectively exfoliated into smaller graphene sheets [50]. The 1.5-hour exfoliation process generates sufficient pressure to expand defect vacancies, ultimately splitting the graphene sheets into smaller lateral sizes [34].

3.5 Particle size analysis

Fig. 8 shows the PSA curve patterns of the graphite raw material and FLG processed via FDE for 1.5 h with 5 wt% Triton X-100 surfactant. The red bars represent the intensity distribution (percentage) based on particle size, while the green line indicates the FDE undersize percentage, representing the cumulative proportion of particles below a specific size [51]. The figure demonstrates that the average lateral size of FLG decreases compared with the raw graphite, confirming the previous TEM analysis results [50]. Fig. 8 (a) indicates the average lateral size of the raw graphite to be approximately ~5.9 µm, with cumulative diameters of 10% = 3.2 µm and 90% = 9.1 µm. Fig. 8 (b) shows the average lateral size of FLG processed via FDE (1.5 h, 5 wt% surfactant) to be 1429.50 ± 299.6 nm, with cumulative diameters of 23% = 1106.43 nm and 90% = 1718.46 nm. These findings

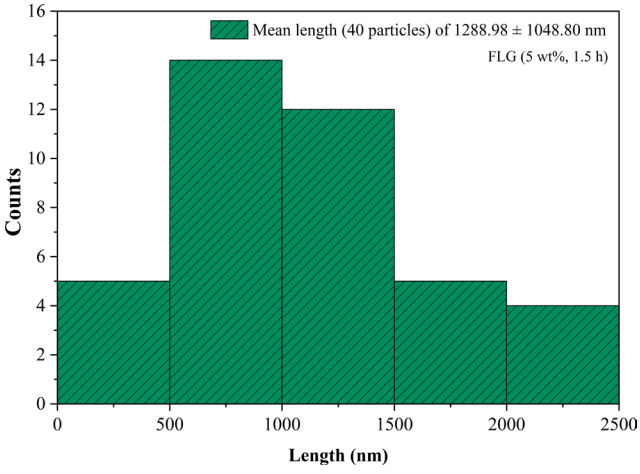

Fig. 7 Flake length histogram for FLG (1.5 h, 5 wt% surfactant)

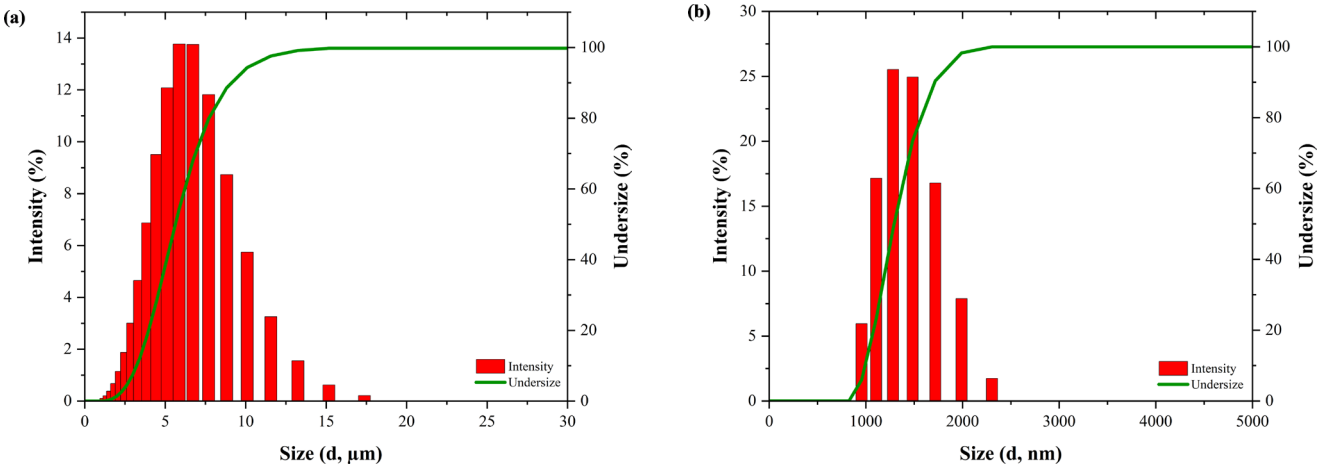

Fig. 8 PSA patterns of (a) Graphite; (b) FLG (1.5 h, 5% surfactant

align with the average lateral particle size of FLG from the TEM analysis (1288.98 ± 1048.80 nm). The average lateral size obtained in this study is also comparable to the lateral size of FLG (<5 layers) synthesized by Zhang et al. [25], reported as 1.9 µm.

Fig. 8 (a) illustrates a broader particle size distribution for graphite with a lower peak, indicating a significant number of particles with non-uniform sizes. Meanwhile, Fig. 8 (b) demonstrates that FLG exhibits a narrower particle size distribution and smaller size range compared with the graphite raw material, suggesting that the particle size of FLG is relatively uniform [52, 53]. A narrow particle size distribution is crucial for maintaining the stability, consistency, and efficiency of nanomaterials in several uses. The performance of nano-based devices enhances with a more uniform nanoparticles size distribution [52–54].

3.6 Fourier transform infrared spectroscopy

Fig. 9 displays the FTIR spectrum of FLG samples (5 wt% surfactant, 1.5 h). A prominent peak at about 3380.11 cm^{-1} is attributed to the stretching and bending vibrations of hydroxyl groups (O–H), signifying the

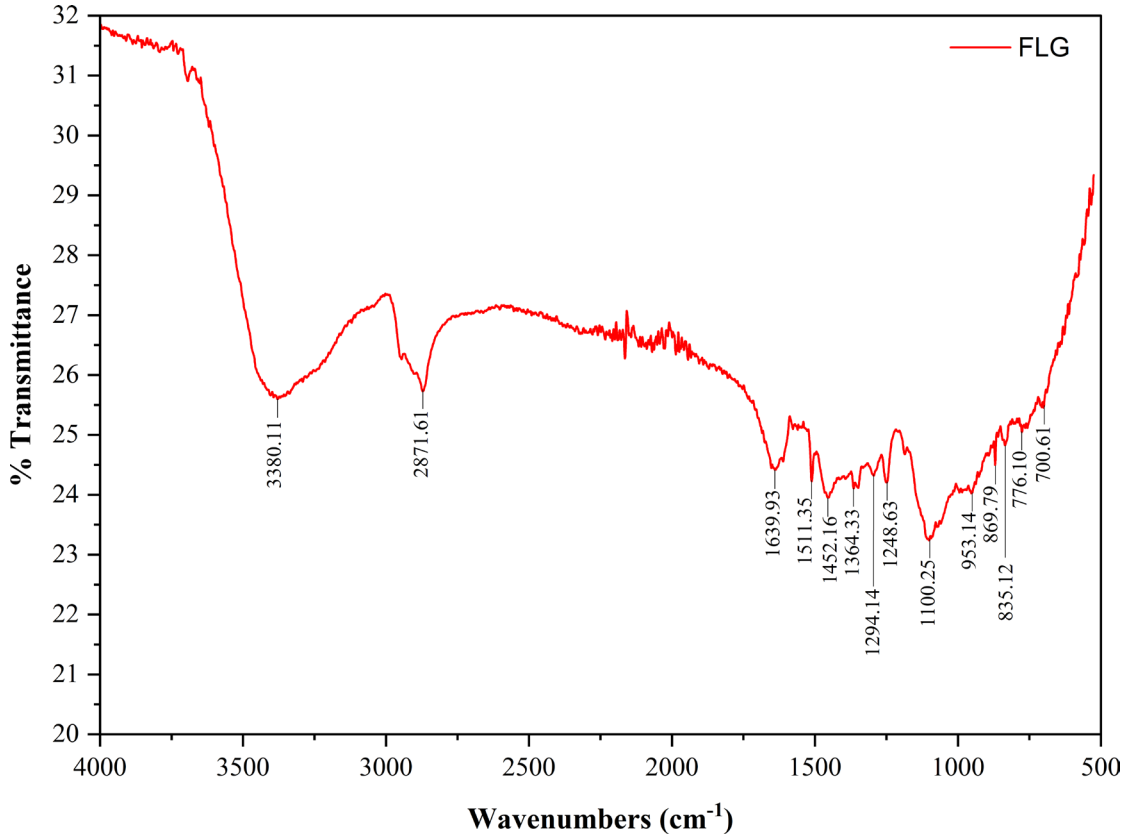

Fig. 9 FTIR spectrum of FLG (1.5 h, 5 wt% surfactant)

existence of physically adsorbed water molecules in the FLG sample [20, 55, 56]. The peak at ~2871.61 cm^{-1} corresponds to the asymmetric and symmetric stretching of aliphatic C–H bonds [20, 55]. Additionally, absorption peaks at about ~1639.93 cm^{-1} and 1511.35 cm^{-1} correspond to the stretching vibrations of C=C groups and bending of C–H bonds in graphene [20, 55, 57, 58]. The band around ~1452.33 cm^{-1} is associated with aromatic groups [59]. Low-intensity wavenumbers at ~1294.14 cm^{-1}, ~1248.63 cm^{-1}, ~1364.33 cm^{-1}, and ~1100.25 cm^{-1} are ascribed to the stretching and bending vibrations of C–O bonds and the asymmetric stretching and bending of C–OH bonds in ether groups (–O–) present in the polyethylene glycol (PEG) chain of the Triton-X surfactant [55, 57, 59–63]. Furthermore, the absorption at ~953.14 cm^{-1} indicates aromatic C–H bond bending in graphene [61]. Peaks at ~869.79 cm^{-1} and 835.12 cm^{-1} represent out-of-plane hydrogen wagging, characteristic of phenyl groups derived from the Triton-X surfactant [62, 63]. Peaks between 850–400 cm^{-1} correspond to heavy-atom bending and rotational motion bands [64]. The FTIR spectrum of the FLG sample (5 wt% surfactant, 1.5 h) confirms that oxidation does not occur during synthesized graphene via the FDE method. This is evidenced by the absence of stretching vibrations of carbonyl groups (C=O) at the zigzag edges, specifically carboxyl groups (–COOH), which typically appear at wavenumbers around ~1720 cm^{-1} [58].

3.7 UV-Vis spectroscopy analysis

Fig. 10 illustrates the UV-Vis absorption spectrum, with the *y*-axis representing absorbance and the *x*-axis denoting the wavelength (nm) of the aqueous FLG solution (5 wt% surfactant, 1.5 h) at different concentrations. Absorbance reflects the amount of light absorbed by the sample at a specific wavelength [65]. The absorption peaks of FLG samples range from 270 to 276 nm, corresponding to the characteristic absorption peaks of graphene nanosheets, typically observed between 270 and 280 nm [66, 67]. These distinct absorption peaks with significant intensity across all concentrations indicate successful graphene exfoliation [67]. The peaks are attributed to π–π^* transitions in the π-conjugated graphene system [67, 68]. The absorption in the 200–230 nm range of the UV-Vis spectrum indicates the presence of Triton X-100 in the sample, consistent with previous studies [69, 70]. This further supports the FTIR analysis, which suggests the presence of Triton surfactant residues on the synthesized FLG, albeit in trace amounts.

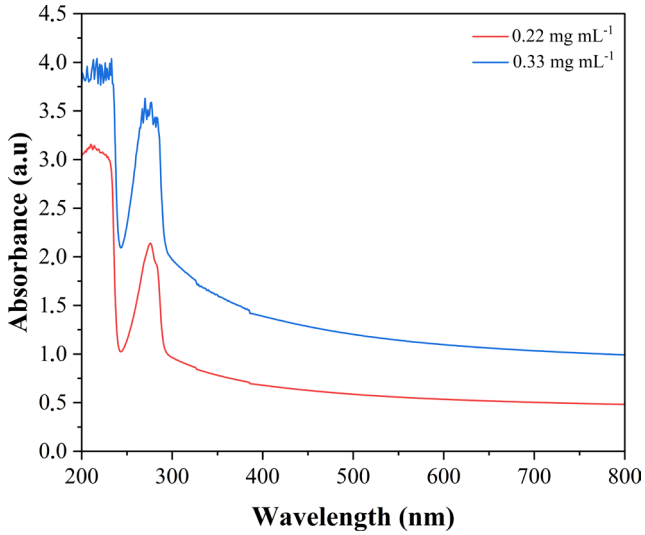

Fig. 10 UV-Vis absorption spectra of FLG (1.5 h, 5 wt% surfactant) in aqueous suspension

Fig. 10 also illustrates that the UV-Vis spectrum intensity increases with increasing concentration, attributable to the enhanced energy absorption by graphene particles [67]. This result aligns with Wang et al. [71], who documented a linear correlation between graphene content and UV-Vis absorbance. This signifies that Lambert-Beer's law is applicable under certain conditions. The law establishes a direct proportional relationship between absorbance and concentration, indicating that an increase in FLG concentration results in a corresponding rise in absorbance, while a reduction in concentration leads to a decrease in absorbance [68, 71, 72]. However, the law becomes less accurate for absorbance values above 1, as the assumption of independent absorbing objects no longer holds. Lambert-Beer's law is mathematically expressed in Eq. (1).

$$A = \varepsilon lc \tag{1}$$

Where A denotes the UV-Vis absorbance, ε represents the molar absorption coefficient associated by the material properties and the wavelength (λ) of the incident light, l (cm) is the path length, and c (mol L^{-1}) is the material concentration [68, 71].

3.8 Mechanism of interaction between Triton X-100 surfactant and graphene

Fig. 11 (a) illustrates the chemical formula of the Triton X-100 surfactant, consisting of a hydrophilic head, the polyethylene oxide chain ($[C_2H_4O]_n$–OH) with $n \approx 9$–10 ethylene oxide units, and a hydrophobic tail, an alkyl chain attached to a benzene ring (C_8H_{17}–C_6H_4) [73]. This surfactant coats nanoscale objects and prevents re-agglomeration by providing steric hindrance between surfactant-coated nanoparticles [74]. In the graphite exfoliation process in

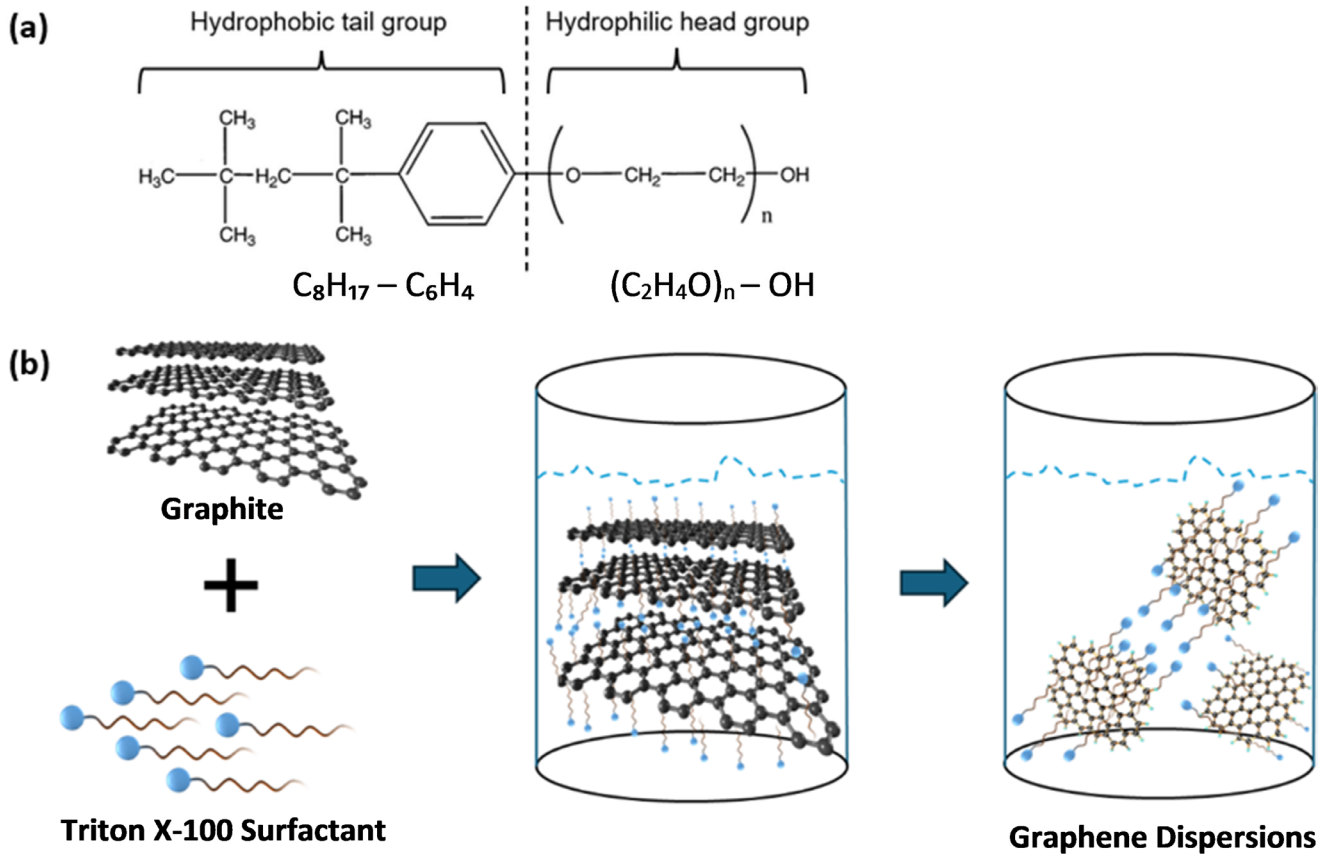

Fig. 11 (a) The chemical structure of the Triton X-100 surfactant with $n \approx 9–10$; (b) Interaction of Triton X-100 surfactant with FLG in an aqueous solution

water, the surfactant diminishes the elevated surface energy of water, enhancing its compatibility with the hydrophobic characteristics of graphite [75]. The surfactant attaches to the graphite surface, creating a stable layer that reduces interfacial energy and enhances its dispersion in water [76].

Fig. 11 (b) illustrates a schematic representation of graphene dispersion and stabilization in an aqueous surfactant solution (Triton X-100). As shown, the non-ionic surfactant Triton X-100 has a hydrophobic tail (C_8H_{17}–C_6H_4) that adsorbs onto graphene flakes through Van der Waals forces and hydrophobic bindings [77–79]. The surface energy of graphene is significantly diminished [46, 74]. Both the hydrophobic tail of Triton X-100 and the graphene surface are non-polar; in an aqueous solution, non-polar molecules tend to interact to minimize contact with polar water molecules [80]. The interaction between the Triton X-100 surfactant and the graphene surface is governed by hydrophobic interactions, aligning the surfactant's tail toward the hydrophobic graphene surface [80, 81]. Furthermore, the hydrophobic tail of the surfactant, consisting of an aromatic alkyl chain (C_8H_{17}–C_6H_4) can engaging in van der Waals association with the graphene surface [80, 81]. Meanwhile, the hydrophilic head ($[C_2H_4O]_n$–OH), which is long and polar, extends into the aqueous medium [46, 74]. The surfactant head contains polyethylene oxide and hydroxyl groups (–OH) with polar characteristics. These groups possess partial positive and negative charges, enabling interactions with polar water molecules. Robust hydrogen bonds may develop between the hydroxyl groups of the surfactant head and water molecules, allowing the head to remain hydrated and dispersed in the aqueous medium [74, 82, 83]. As two graphene flakes covered with Triton X-100 surfactant approach each other, the protruding hydrophilic groups interact, generating osmotic repulsion forces between the graphene layers [74]. The steric hindrance created by the long hydrophilic segment of Triton X-100 prevents graphene aggregation during shear mixing [74]. The non-ionic surfactant Triton X-100 has low electrical potential, and its stabilization mechanism relies on steric hindrance. This hindrance establishes an energy barrier that prevents graphene aggregation, thereby enhancing its stability in aqueous solutions [40]. Consequently, graphene layers remain stably dispersed in water due to steric hindrance between surrounding graphene sheets, which overcomes van der Waals attraction forces [84].

Fig. 12 illustrates the synthesis mechanism of graphene using the FDE method. The inclusion of surfactants to

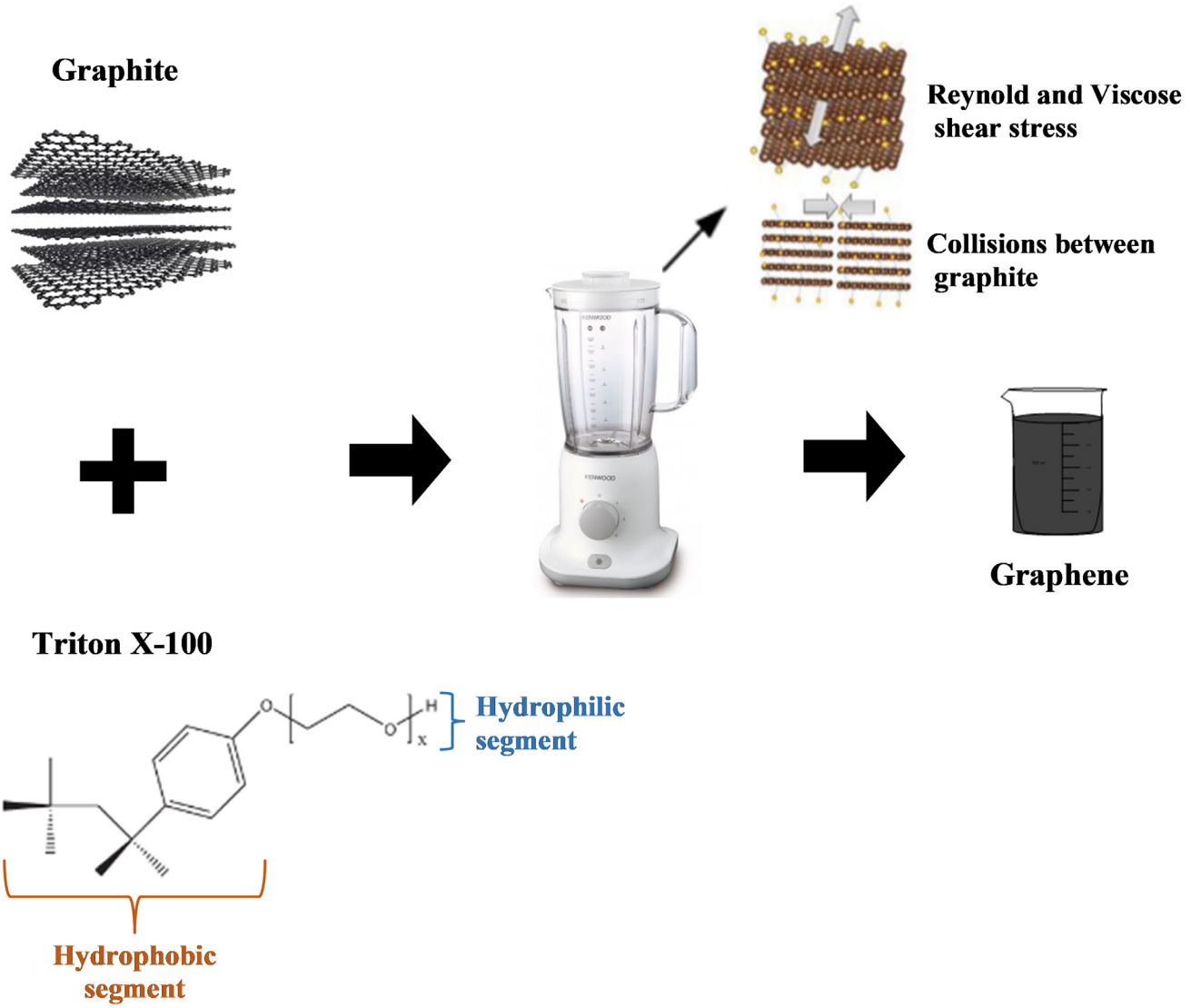

Fig. 12 The mechanism for producing FLG using the FDE method

graphite diminishes the potential energy between adjacent layers. Turbulence produced in the blender ($Re_{blade} = 10^6$ and $\gamma_t \approx 2.8 \times 10^4\ s^{-1}$, where Re is the Reynolds number (dimensionless) and γ_t is the turbulance shear rate) [12, 20], along with viscous shear stress, Reynolds shear stress, and particle collisions facilitates the exfoliation of graphite into graphene [19, 20]. Consequently, graphite with up to 4 layers is dispersed uniformly in the aqueous solution.

4 Conclusion

Low-defect FLG, predominantly consisting of ~4 layers, was effectively synthesized using a simple, economical, and eco-friendly FDE method. The FDE process was conducted in a rotating blade mixer (kitchen blender) with water as the working fluid and Triton-X surfactant at varying concentrations (1 wt% to 5 wt%) and processing durations (0.5 to 1.5 h). Higher surfactant concentrations enhanced the graphene stability, resulting in uniformly dispersed exfoliated graphene in the aqueous solution. Longer FDE process times reduced defects in the graphene, as extended exfoliation allowed defect vacancies to grow, promoting more complete exfoliation of graphene layers. RS analysis revealed that the optimal FLG sample was obtained with a 5 wt% surfactant concentration and a processing time of 1.5 h, yielding low-defect FLG dominated by ~4-layer graphene (4LG), as indicated by three Lorentzian components in the 2D peak curve fitting. The resulting FLG samples exhibited D band to G band intensity ratios (I_D/I_G) ranging from 0.02 to 0.11 and 2D band to G band intensity ratios (I_{2D}/I_G) between 0.18 and 0.30. Raman imaging confirmed that the produced FLG predominantly exhibited armchair edge chirality over zigzag edges, signifying the existence of edge defects. TEM

investigation verified the existence of FLG with average flake length of approximately 1288.98 ± 1048.80 nm. PSA demonstrated that FLG exhibited a narrower particle size distribution and lower dimensions than the raw graphite material, with an average lateral size of 1429.50 ± 299.6 nm, indicating relatively uniform particle size. FTIR spectroscopy showed that the defects in the FLG were attributed to edge and vacancy defects formed during exfoliation rather than oxidation. UV-Vis spectroscopy indicated absorption peaks between 270 nm and 276 nm, corresponding to graphene nanosheets. Although FLG still contained trace amounts of surfactant, Triton X-100 effectively produced graphene with a low defect level.

Acknowledgment

This work was supported by the Ministry of Education, Culture, Research, and Technology Republic of Indonesia via the Riset Terapan scheme (contract number: 20687/UN19.5.1.3/AL.04/2024).

References

[1] Wei, W., Qu, X. "Extraordinary Physical Properties of Functionalized Graphene", Small, 8(14), pp. 2138–2151, 2012. https://doi.org/10.1002/smll.201200104

[2] Brownson, D. A. C., Banks, C. E. "Graphene Electrochemistry: An Overview of Potential Applications", Analyst, 135(11), pp. 2768–27778, 2010. https://doi.org/10.1039/c0an00590h

[3] Qiao, Y., Li, X., Hirtz, T., Deng, G., Wei, Y., …, Ren, T.-L. "Graphene-based Wearable Sensors", Nanoscale, 11(41), pp. 18923–18945, 2019. https://doi.org/10.1039/C9NR05532K

[4] Kaur, K., Singh, J., Kaur, M. "Compressive Strength of Rice Husk Ash Based Geopolymer: The Effect of Alkaline Activator", Construction and Building Materials, 169, pp. 188–192, 2018. https://doi.org/10.1016/j.conbuildmat.2018.02.200

[5] Yu, X., Lin, D., Li, P., Su, Z. "Recent Advances in the Synthesis and Energy Applications of TiO_2-graphene Nanohybrids", Solar Energy Materials and Solar Cells, 172, pp. 252–269, 2017. https://doi.org/10.1016/j.solmat.2017.07.045

[6] Ferrari, A. C., Basko, D. M. "Raman Spectroscopy as a Versatile Tool for Studying the Properties of Graphene", Nature Nanotechnology, 8(4), pp. 235–246, 2013. https://doi.org/10.1038/nnano.2013.46

[7] Nicolosi, V., Chhowalla, M., Kanatzidis, M. G., Strano, M. S., Coleman, J. N. "Liquid Exfoliation of Layered Materials", Science, 340(6139), 1226419, 2013. https://doi.org/10.1126/science.1226419

[8] Zhang, D., Du, X., Shi, L., Gao, R. "Shape-controlled Synthesis and Catalytic Application of Ceria Nanomaterials", Dalton Transactions, 41(48), pp. 14455–14475, 2012. https://doi.org/10.1039/c2dt31759a

[9] Narayan, R., Kim, S. O. "Surfactant Mediated Liquid Phase Exfoliation of Graphene", Nano Convergence, 2(1), 20, 2015. https://doi.org/10.1186/s40580-015-0050-x

[10] Gao, Y., Zhang, Y., Yang, Y., Zhang, J., Gu, F. "Molecular Dynamics Investigation of Interfacial Adhesion between Oxidised Bitumen and Mineral Surfaces", Applied Surface Science, 479, pp. 449–462, 2019. https://doi.org/10.1016/j.apsusc.2019.02.121

[11] Hernandez, Y., Nicolosi, V., Lotya, M., Blighe, F. M., Sun, Z., …, Coleman, J. N. "High-yield Production of Graphene by Liquid-phase Exfoliation of Graphite", Nature Nanotechnology, 3(9), pp. 563–568, 2008. https://doi.org/10.1038/nnano.2008.215

[12] Varrla, E., Paton, K. R., Backes, C., Harvey, A., Smith, R. J., McCauley, J., Coleman, J. N. "Turbulence-assisted Shear Exfoliation of Graphene Using Household Detergent and a Kitchen Blender", Nanoscale, 6(20), pp. 11810–11819, 2014. https://doi.org/10.1039/c4nr03560g

[13] Paton, K. R., Varrla, E., Backes, C., Smith, R. J., Khan, U., …, Coleman, J. N. "Scalable Production of Large Quantities of Defect-free Few-layer Graphene by Shear Exfoliation in Liquids", Nature Materials, 13(6), pp. 624–630, 2014. https://doi.org/10.1038/nmat3944

[14] Chen, K., Xue, D. "Preparation of Colloidal Graphene in Quantity by Electrochemical Exfoliation", Journal of Colloid and Interface Science, 436, pp. 41–46, 2014. https://doi.org/10.1016/j.jcis.2014.08.057

[15] Stafford, J., Patapas, A., Uzo, N., Matar, O. K., Petit, C. "Towards Scale-up of Graphene Production via Nonoxidizing Liquid Exfoliation Methods", AIChE Journal, 64(9), pp. 3246–3276, 2018. https://doi.org/10.1002/aic.16174

[16] Xu, Y., Cao, H., Xue, Y., Li, B., Cai, W. "Liquid-Phase Exfoliation of Graphene: An Overview on Exfoliation Media, Techniques, and Challenges", Nanomaterials, 8(11), 942, 2018. https://doi.org/10.3390/nano8110942

[17] Guardia, L., Fernández-Merino, M. J., Paredes, J. I., Solís-Fernández, P., Villar-Rodil, S., Martínez-Alonso, A., Tascón, J. M. D. "High-throughput Production of Pristine Graphene in an Aqueous Dispersion Assisted by Non-ionic Surfactants", Carbon, 49(5), pp. 1653–1662, 2011. https://doi.org/10.1016/j.carbon.2010.12.049

[18] Narayan, R., Lim, J., Jeon, T., Li, D. J., Kim, S. O. "Perylene Tetracarboxylate Surfactant Assisted Liquid Phase Exfoliation of Graphite into Graphene Nanosheets with Facile Re-dispersibility in Aqueous/Organic Polar Solvents", Carbon, 119, pp. 555–568, 2017. https://doi.org/10.1016/j.carbon.2017.04.071

[19] Yi, M., Shen, Z. "Kitchen Blender for Producing High-quality Few-layer Graphene", Carbon, 78, pp. 622–626, 2014. https://doi.org/10.1016/j.carbon.2014.07.035

[20] Amri, A., Bertilsya Hendri, Y., Yin, C.-Y., Mahbubur Rahman, M., Altarawneh, M., Jiang, Z.-T. "Very-few-layer Graphene Obtained from Facile Two-step Shear Exfoliation in Aqueous Solution", Chemical Engineering Science, 245, 116848, 2021. https://doi.org/10.1016/j.ces.2021.116848

[21] Wang, S., Yi, M., Shen, Z. "The Effect of Surfactants and their Concentration on the Liquid Exfoliation of Graphene", RSC Advances, 6(61), pp. 56705–56710, 2016. https://doi.org/10.1039/c6ra10933k

[22] Girish, S., Tambe, P. "Surfactant Assisted Exfoliation of High Purity Graphene in Aqueous Solution as a Nanofluid Using Kitchen Blender: Influence on Dispersion, Thermal Conductivity and Rheological Properties", Advanced Powder Technology, 33(10), 103767, 2022. https://doi.org/10.1016/j.apt.2022.103767

[23] OriginLab "OriginPro, (Version 2025 (10.2))", [computer program] Available at: https://www.originlab.com/index.aspx?go=Products/Origin [Accessed: 08 September 2025]

[24] Bharti Airtel Ltd. "ImageJ, (Version 1.52v)", [computer program] Available at: https://imagej.en.softonic.com/ [Accessed: 06 September 2025]

[25] Zhang, Z., Jin, H., Wu, C., Ji, J. "Efficient Production of High-Quality Few-Layer Graphene Using a Simple Hydrodynamic-Assisted Exfoliation Method", Nanoscale Research Letters, 13(1), 416, 2018. https://doi.org/10.1186/s11671-018-2830-9

[26] Malard, L. M., Pimenta, M. A., Dresselhaus, G., Dresselhaus, M. S. "Raman Spectroscopy in Graphene", Physics Reports, 473(5–6), pp. 51–87, 2009. https://doi.org/10.1016/j.physrep.2009.02.003

[27] Roscher, S., Hoffmann, R., Ambacher, O. "Determination of the Graphene-graphite Ratio of Graphene Powder by Raman 2D Band Symmetry Analysis", Analytical Methods, 11(9), pp. 1224–1228, 2019. https://doi.org/10.1039/c8ay02619j

[28] Jibrael, R. I., Mohammed, M. K. A. "Production of Graphene Powder by Electrochemical Exfoliation of Graphite Electrodes Immersed in Aqueous Solution", Optik, 127(16), pp. 6384–6389, 2016. https://doi.org/10.1016/j.ijleo.2016.04.101

[29] Cong, C., Yu, T., Saito, R., Dresselhaus, G. F., Dresselhaus, M. S. "Second-Order Overtone and Combination Raman Modes of Graphene Layers in the Range of 1690–2150 cm^{-1}", ACS Nano, 5(3), pp. 1600–1605, 2011. https://doi.org/10.1021/nn200010m

[30] Ferrari, A. C., Meyer, J. C., Scardaci, V., Casiraghi, C., Lazzeri, M., …, Geim, A. K. "Raman Spectrum of Graphene and Graphene Layers", Physical Review Letters, 97(18), 187401, 2006. https://doi.org/10.1103/PhysRevLett.97.187401

[31] You, Y., Ni, Z., Yu, T., Shen, Z. "Edge Chirality Determination of Graphene by Raman Spectroscopy", Applied Physical Letters, 93(16), 163112, 2008. https://doi.org/10.1063/1.3005599

[32] Yi, M., Shen, Z. "Fluid Dynamics: An Emerging Route for the Scalable Production of Graphene in the Last Five Years", RSC Advances, 6(76), pp. 72525–72536, 2016. https://doi.org/10.1039/c6ra15269d

[33] Liu, L., Qing, M., Wang, Y., Chen, S. "Defects in Graphene: Generation, Healing, and Their Effects on the Properties of Graphene: A Review", Journal of Materials Science & Technology, 31(6), pp. 599–606, 2015. https://doi.org/10.1016/j.jmst.2014.11.019

[34] Ganesan, K., Ghosh, S., Gopala Krishna, N., Ilango, S., Kamruddin, M., Tyagi, A. K. "A Comparative Study on Defect Estimation Using XPS and Raman Spectroscopy in Few Layer Nanographitic Structures", Physical Chemistry Chemical Physics, 18(32), pp. 22160–22167, 2016. https://doi.org/10.1039/c6cp02033j

[35] Poutrel, Q.-A., Wang, Z., Wang, D., Soutis, C., Gresil, M. "Effect of Pre and Post-Dispersion on Electro-Thermo-Mechanical Properties of a Graphene Enhanced Epoxy", Applied Composite Materials, 24(2), pp. 313–336, 2017. https://doi.org/10.1007/s10443-016-9541-0

[36] Nguyen, V. T., Le, H. D., Nguyen, V. C., Tam Ngo, T. T., Le, D. Q., Nguyen, X. N., Phan, N. M. "Synthesis of Multi-layer Graphene Films on Copper Tape by Atmospheric Pressure Chemical Vapor Deposition Method", Advances in Natural Sciences: Nanoscience and Nanotechnology, 4(3), 035012, 2013. https://doi.org/10.1088/2043-6262/4/3/035012

[37] Huang, H., Zhou, F., Lu, P., Li, X., Das, P., Feng, X., Müllen, K., Wu, Z.-S. "Design and Construction of Few-layer Graphene Cathode for Ultrafast and High-capacity Aluminum-ion Batteries", Energy Storage Materials, 27, pp. 396–404, 2020. https://doi.org/10.1016/j.ensm.2020.02.011

[38] Phiri, J., Gane, P., Maloney, T. C. "High-concentration Shear-exfoliated Colloidal Dispersion of Surfactant–polymer-stabilized Few-layer Graphene Sheets", Journal of Materials Science, 52(13), pp. 8321–8337, 2017. https://doi.org/10.1007/s10853-017-1049-y

[39] Kaur, A., Morton, J. A., Tyurnina, A. V., Priyadarshi, A., Holland, A., Mi, J., Porfyrakis, K., Eskin, D. G., Tzanakis, I. "Temperature as a Key Parameter for Graphene Sono-exfoliation in Water", Ultrasonics Sonochemistry, 90, 106187, 2022. https://doi.org/10.1016/j.ultsonch.2022.106187

[40] Nazari, B., Ranjbar, Z., Hashjin, R. R., Rezvani Moghaddam, A., Momen, G., Ranjbar, B. "Dispersing Graphene in Aqueous Media: Investigating the Effect of Different Surfactants", Colloids and Surfaces A: Physicochemical and Engineering Aspects, 582, 123870, 2019. https://doi.org/10.1016/j.colsurfa.2019.123870

[41] Tang, B., Guoxin, H., Gao, H. "Raman Spectroscopic Characterization of Graphene", Applied Spectroscopy Reviews, 45(5), pp. 369–407, 2010. https://doi.org/10.1080/05704928.2010.483886

[42] Graf, D., Molitor, F., Ensslin, K., Stampfer, C., Jungen, A., Hierold, C., Wirtz, L. "Spatially Resolved Raman Spectroscopy of Single- and Few-Layer Graphene", Nano Letters, 7(2), pp. 238–242, 2007. https://doi.org/10.1021/nl061702a

[43] Wang, Y. Y., Ni, Z. H., Shen, Z. X., Wang, H. M., Wu, Y. H. "Interference Enhancement of Raman Signal of Graphene", Applied Physics Letters, 92(4), 043121, 2008. https://doi.org/10.1063/1.2838745

[44] Koskinen, P., Malola, S., Häkkinen, H. "Evidence for Graphene Edges beyond Zigzag and Armchair", Physical Review B, 80(7), 073401, 2009. https://doi.org/10.1103/PhysRevB.80.073401

[45] Gürünlü, B., Taşdelen-Yücedağ, Ç., Bayramoğlu, M. "Graphene Synthesis by Ultrasound Energy-Assisted Exfoliation of Graphite in Various Solvents", Crystals, 10(11), 1037, 2020. https://doi.org/10.3390/cryst10111037

[46] Javadian, S., Kakemam, J. "Intermicellar Interaction in Surfactant Solutions; a Review Study", Journal of Molecular Liquids, 242, pp. 115–128, 2017. https://doi.org/10.1016/j.molliq.2017.06.117

[47] Tyurnina, A. V., Tzanakis, I., Morton, J., Mi, J., Porfyrakis, K., Maciejewska, B. M., Grobert, N., Eskin, D. G. "Ultrasonic Exfoliation of Graphene in Water: A Key Parameter Study", Carbon, 168, pp. 737–747, 2020. https://doi.org/10.1016/j.carbon.2020.06.029

[48] Lotya, M., King, P. J., Khan, U., De, S., Coleman, J. N. "High-Concentration, Surfactant-Stabilized Graphene Dispersions", ACS Nano, 4(6), pp. 3155–3162, 2010. https://doi.org/10.1021/nn1005304

[49] Khan, U., O'Neill, A., Porwal, H., May, P., Nawaz, K., Coleman, J. N. "Size Selection of Dispersed, Exfoliated Graphene Flakes by Controlled Centrifugation", Carbon, 50(2), pp. 470–475, 2012. https://doi.org/10.1016/j.carbon.2011.09.001

[50] Turner, P., Hodnett, M., Dorey, R., Carey, J. D. "Controlled Sonication as a Route to *in-situ* Graphene Flake Size Control", Scientific Reports, 9(1), 8710, 2019. https://doi.org/10.1038/s41598-019-45059-5

[51] Wang, Y., He, Y., Zhan, J., Li, Z. "Identification of Soil Particle Size Distribution in Different Sedimentary Environments at River Basin Scale by Fractal Dimension", Scientific Reports, 12(1), 10960, 2022. https://doi.org/10.1038/s41598-022-15141-6

[52] Burlakov, V., Goriely, A. "Thermodynamic Limit for Particle Monodispersity: How Narrow Can a Particle Size Distribution Be?", Europhysics Letters, 119(5), 50001, 2017. https://doi.org/10.1209/0295-5075/119/50001

[53] Bertran, A., Sandoval, S., Oró-Solé, J., Sánchez, À., Tobias, G. "Particle Size Determination from Magnetization Curves in Reduced Graphene Oxide Decorated with Monodispersed Superparamagnetic Iron Oxide Nanoparticles", Journal of Colloid and Interface Science, 566, pp. 107–119, 2020. https://doi.org/10.1016/j.jcis.2020.01.072

[54] Li, Y., Park, C.-W. "Particle Size Distribution in the Synthesis of Nanoparticles Using Microemulsions", Langmuir, 15(4), pp. 952–956, 1999. https://doi.org/10.1021/la980550z

[55] Tavakoli, F., Salavati-Niasari, M., badiei, A., Mohandes, F. "Green Synthesis and Characterization of Graphene Nanosheets", Materials Research Bulletin, 63, pp. 51–57, 2015. https://doi.org/10.1016/j.materresbull.2014.11.045

[56] Kumar, M. M., Nagesh, G. V., Deepthi, S., Ravikiran, Y. T., Patil, D., Revanasiddappa, M., Manjunath, S. "Dielectric Response and Electric Modulus Studies of Polythiophene/Reduced Graphene Oxide Nanocomposites", Materials Science Forum, 1099, pp. 69–74, 2023. https://doi.org/10.4028/p-Nx1nnA

[57] Lin, J.-H. "The Anionic Surfactant/Ionic Liquids Intercalated Reduced Graphene Oxide for High-performance Supercapacitors", Nanoscale Research Letters, 13(1), 215, 2018. https://doi.org/10.1186/s11671-018-2636-9

[58] Kar, T., Scheiner, S., Adhikari, U., Roy, A. K. "Site Preferences of Carboyxl Groups on the Periphery of Graphene and Their Characteristic IR Spectra", The Journal of Physical Chemistry C, 117(35), pp. 18206–18215, 2013. https://doi.org/10.1021/jp403728b

[59] Pfaffeneder-Kmen, M., Casas, I. F., Naghilou, A., Trettenhahn, G., Kautek, W. "A Multivariate Curve Resolution Evaluation of an *in-situ* ATR-FTIR Spectroscopy Investigation of the Electrochemical Reduction of Graphene Oxide", Electrochim Acta, 255, pp. 160–167, 2017. https://doi.org/10.1016/j.electacta.2017.09.124

[60] Shirota, H., Kakinuma, S., Itoyama, Y., Umecky, T., Takamuku, T. "Effects of Tetrafluoroborate and Bis(trifluoromethylsulfonyl) amide Anions on the Microscopic Structures of 1-Methyl-3-octylimidazolium-Based Ionic Liquids and Benzene Mixtures: A Multiple Approach by ATR-IR, NMR, and Femtosecond Raman-Induced Kerr Effect Spectroscopy", The Journal of Physical Chemistry B, 120(3), pp. 513–526, 2016. https://doi.org/10.1021/acs.jpcb.5b10917

[61] Hayyan, M., Abo-Hamad, A., AlSaadi, M. A., Hashim, M. A. "Functionalization of Graphene Using Deep Eutectic Solvents", Nanoscale Research Letters, 10(1), 324, 2015. https://doi.org/10.1186/s11671-015-1004-2

[62] Fontana, A., Guernelli, S., Di Crescenzo, A., Di Profio, P., Palomba, F., De Crescentini, L., Baschieri, A., Amorati, R. "Cardanol-like Co-surfactants Solubilized in Pegylated Micelles Keep their Antioxidant Activity and Preserve Polyethylene Glycol Chains from Oxidation", Journal of Molecular Liquids, 293, 111465, 2019. https://doi.org/10.1016/j.molliq.2019.111465

[63] Si, Y., Samulski, E. T. "Synthesis of Water Soluble Graphene", Nano Letters, 8(6), pp. 1679–1682, 2008. https://doi.org/10.1021/nl080604h

[64] Kruer-Zerhusen, N., Cantero-Tubilla, B., Wilson, D. B. "Characterization of Cellulose Crystallinity after Enzymatic Treatment Using Fourier Transform Infrared Spectroscopy (FTIR)", Cellulose, 25(1), pp. 37–48, 2018. https://doi.org/10.1007/s10570-017-1542-0

[65] Suliman, R. T. "Evaluation of the Absorbance and Transmittance of the Optical Light for Three Different Types of Composite Resin Stored in Artificial Saliva (in vitro Study)", Al-Rafidain Dental Journal, 17(1), pp. 86–97, 2017. https://doi.org/10.33899/rden.2016.164142

[66] Krishnamoorthy, K., Kim, G.-S., Kim, S. J. "Graphene Nanosheets: Ultrasound Assisted Synthesis and Characterization", Ultrasonics Sonochemistry, 20(2), pp. 644–649, 2013. https://doi.org/10.1016/j.ultsonch.2012.09.007

[67] Abdul Rahim, M. A. H., Samsurrijal, S. F., Abdullah, A. A.-A., Mohd Noor, S. N. F. "UV–Vis Spectroscopic Trends of Liquid-exfoliated Graphite/Graphene Nanoplatelets/Bioactive Glass Mixtures", Journal of Physical Science, 34(2), pp. 1–12, 2023. https://doi.org/10.21315/jps2023.34.2.1

[68] Vacacela Gomez, C., Guevara, M., Tene, T., Villamagua, L., Usca, G. T., Maldonado, F., Tapia, C., Cataldo, A., Bellucci, S., Caputi, L. S. "The Liquid Exfoliation of Graphene in Polar Solvents", Applied Surface Science, 546, 149046, 2021. https://doi.org/10.1016/j.apsusc.2021.149046

[69] Tiller, G. E., Mueller, T. J., Dockter, M. E., Struve, W. G. "Hydrogenation of Triton X-100 Eliminates its Fluorescence and Ultraviolet Light Absorption while Preserving its Detergent Properties", Analytical Biochemistry, 141(1), pp. 262–266, 1984. https://doi.org/10.1016/0003-2697(84)90455-X

[70] Pavlović, B., Cvijetić, N., Dragačević, L., Ivković, B., Vujić, Z., Kuntić, V. "Direct UV Spectrophotometry and HPLC Determination of Triton X-100 in Split Virus Influenza Vaccine", Journal of AOAC International, 99(2), pp. 396–400, 2016. https://doi.org/10.5740/jaoacint.15-0201

[71] Wang, G., Shen, X., Wang, B., Yao, J., Park, J. "Synthesis and Characterisation of Hydrophilic and Organophilic Graphene Nanosheets", Carbon, 47(5), pp. 1359–1364, 2009. https://doi.org/10.1016/j.carbon.2009.01.027

[72] Huang, G., He, J., Zhang, X., Feng, M., Tan, Y., Lv, C., Huang, H., Jin, Z. "Applications of Lambert-Beer Law in the Preparation and Performance Evaluation of Graphene Modified Asphalt", Construction and Building Materials, 273, 121582, 2021. https://doi.org/10.1016/j.conbuildmat.2020.121582

[73] Kaur, P., Shin, M.-S., Sharma, N., Kaur, N., Joshi, A., Chae, S.-R., Park, J.-S., Kang, M.-S., Sekhon, S. S. "Non-covalent Functionalization of Graphene with Poly(diallyl dimethylammonium) Chloride: Effect of a Non-ionic Surfactant", International Journal of Hydrogen Energy, 40(3), pp. 1541–1547, 2015. https://doi.org/10.1016/j.ijhydene.2014.11.068

[74] Smith, R. J., Lotya, M., Coleman, J. N. "The Importance of Repulsive Potential Barriers for the Dispersion of Graphene Using Surfactants", New Journal of Physics, 12(12), 125008, 2010. https://doi.org/10.1088/1367-2630/12/12/125008

[75] Sharma, V., Garg, A., Sood, S. C. "Graphene Synthesis via Exfoliation of Graphite by Ultrasonication", International Journal of Engineering Trends and Technology, 26(1), pp. 37–42, 2015. https://doi.org/10.14445/22315381/IJETT-V26P208

[76] Doganci, M. D., Cavusoglu, S., Oksuz, M., Erbil, H. Y. "Effect of Surface Free Energy to Control the Deposit Morphology during Evaporation of Graphite/SDS Dispersion Drops", Colloids and Surfaces A: Physicochemical and Engineering Aspects, 461, pp. 310–322, 2014. https://doi.org/10.1016/j.colsurfa.2014.08.004

[77] Zhang, F., Li, S., Zhang, Q., Liu, J., Zeng, S., Liu, M., Sun, D. "Adsorption of Different Types of Surfactants on Graphene Oxide", Journal of Molecular Liquids, 276, pp. 338–346, 2019. https://doi.org/10.1016/j.molliq.2018.12.009

[78] Bai, Y., Lin, D., Wu, F., Wang, Z., Xing, B. "Adsorption of Triton X-series Surfactants and its Role in Stabilizing Multi-walled Carbon Nanotube Suspensions", Chemosphere, 79(4), pp. 362–367, 2010. https://doi.org/10.1016/j.chemosphere.2010.02.023

[79] Kaur, P., Shin, M.-S., Park, J.-S., Verma, G., Sekhon, S. S. "Supramolecular Modification of Carbon Nanofibers with Poly(diallyl dimethylammonium) Chloride and Triton X-100 for Electrochemical Application", International Journal of Hydrogen Energy, 43(13), pp. 6575–6585, 2018. https://doi.org/10.1016/j.ijhydene.2018.02.075

[80] Bhardwaj, V., Chauhan, S., Sharma, K., Sharma, P. "Cosmeceutical Active Molecules and Ethoxylated Alkylphenol (Triton X-100) in Hydroalcoholic Solutions: Transport Properties Examination", Thermochimica Acta, 577, pp. 66–78, 2014. https://doi.org/10.1016/j.tca.2013.12.014

[81] Zhang, C., Zhao, X., Lei, J., Ma, Y., Du, F. "The Wetting Behavior of Aqueous Surfactant Solutions on Wheat (*Triticum aestivum*) Leaf Surfaces", Soft Matter, 13(2), pp. 503–513, 2017. https://doi.org/10.1039/C6SM02387H

[82] Kumar, N., Maldarelli, C., Couzis, A. "An Infrared Spectroscopy Study of the Hydrogen Bonding and Water Restructuring as a Trisiloxane Superspreading Surfactant Adsorbs onto an Aqueous–hydrophobic Surface", Colloids and Surfaces A: Physicochemical and Engineering Aspects, 277(1–3), pp. 98–106, 2006. https://doi.org/10.1016/j.colsurfa.2005.11.040

[83] Liu, S., Wang, X., Chen, L., Hou, L., Zhou, T. "Aggregation Morphologies of a Series of Heterogemini Surfactants with a Hydroxyl Head Group in Aqueous Solution", Soft Matter, 10(45), pp. 9177–9186, 2014. https://doi.org/10.1039/C4SM01524J

[84] Zhang, K., Zhang, X., Li, H., Xing, X., Jin, L., Cao, Q., Li, P. "Direct Exfoliation of Graphite into Graphene in Aqueous Solution Using a Novel Surfactant Obtained from Used Engine Oil", Journal of Materials Science, 53(4), pp. 2484–2496, 2018. https://doi.org/10.1007/s10853-017-1729-7